Interstitial Oxygen in Perovskite-Related $Sr_{6-2x}Nb_{2+2x}O_{11+3x}$

Man-Rong Li and Seung-Tae Hong*

LG Chem Research Park, Daejeon 305-380, South Korea

Received November 29, 2007. Revised Manuscript Received January 22, 2008

Solid solutions of perovskite-related compounds $Sr_{6-2x}Nb_{2+2x}O_{11+3x}$($0.103 \le x \le 0.333$) were synthesized at 1523 K in air. The crystal structures were determined and refined by a combined powder X-ray and neutron Rietveld method ($Fm\bar{3}m$, $a = 8.3103$Å, $Z = 2$, $R_p = 4.02\%$, $wR_p = 5.63\%$, $\chi^2 = 4.44$, 23 °C, for example, with $x = 0.103$). According to the Fourier synthesis map analysis, a new structural model, which includes interstitial oxygen, is proposed for the title compounds. The metal atoms fully occupy the A or B-sites of the perovskite (ABO_3) structure. The pure Nb site and the mixed Sr/Nb site form a rock-salt type ordering in the B-site. The oxygen atoms and anionic vacancies are distributed statistically over the normal (O1 at 24*e* site) and interstitial positions (O2 at 48*h* site), and the occupancies for the interstitial sites are 8.5–15.4%. According to the electrical conductivities as functions of temperature and oxygen partial pressure under dry and wet air, the compounds are predominant oxide ion conductors at high temperatures and proton conductors as well at lower temperatures under wet air. The total conductivity increases with increasing strontium content, or decreasing oxygen content but increasing site occupancy at the interstitial oxygen site.

1. Introduction

Materials with the oxygen-deficient perovskite structure ABO_{3-y} have received considerable attention because of their potential applications in the area of solid oxide fuel cells.[1–4] The high tolerance of the perovskite structure in both A- and B-sublattices promotes the incorporation of multiple cations with different valences and sizes, which results in various superstructures. A double superstructure is known for the $AA'BB'O_6$ type composition, or in general for a multiple occupation of the A or B sublattices through cation ordering.[5,6] The cryolite structure A_3BO_6 is another example of double perovskites of A_2ABO_6 type. A proper variation of composition in the B sublattice for given oxidation states of metal ions allows a variation of oxygen deficiency in the structures. It is the case for $A^{II}_4(A^{II}_{2-2x}B^{V}_{2+2x})O_{11+3x}$ or $A^{II}_{6-2x}B^{V}_{2+2x}O_{11+3x}$ type structures, where A represents alkaline earth metals and B niobium or tantalum atoms.[7–19] Many of these compounds displayed predominant oxide ion conductivity at high temperatures,[10–15] as well as a proton conductivity at lower temperatures under wet atmospheres.[14–16]

A simple and typical but oxygen-deficient cubic cryolite structure was proposed for the series of compounds $Sr_{6-2x}B_{2+2x}O_{11+3x}$ (B = Nb or Ta) since the initial study[7] on $Sr_6Ta_2O_{11}$. However, Rietveld refinements for $Sr_{5.92}Ta_{2.08}O_{11.12}$,[16] $Sr_{5.6}Ta_{2.4}O_{11.6}$,[17] and $Sr_4Nb_2O_9$ (= $Sr_{5.333}Nb_{2.667}O_{12}$)[18] resulted in poor profile fits and abnormal atomic displacement parameters (ADPs) when the typical cryolite structure was assumed, implying some problems with the crystal structure. To justify it, modulated structures in atomic positions or in chemical compositions were proposed by electron crystallography.[17] Two other approaches, a non-harmonicity on ADPs[18] or positional disorders for A-site Sr and oxygen ions,[19] were also developed to better explain X-ray and neutron diffraction data. However, no conclusive structural model has been developed. Here we present detailed crystal structure refinement results and electrical conductivities of $Sr_{6-2x}Nb_{2+2x}O_{11+3x}$ ($0.103 \le x \le 0.333$). According to the combined powder X-ray and neutron diffraction analysis, a new structural model is proposed, which includes interstitial oxide ions in the perovskite-related structure.

* Corresponding author. E-mail: sthong@lgchem.com. Phone: (82) 42-866-2498. Fax: (82) 42-861-2057.

(1) Goodenough, J. B. *Nature* **2000**, *404*, 821.
(2) Boukamp, B. A. *Nat. Mater.* **2003**, *2*, 294.
(3) Ruiz-Morales, J. C.; Canales-Vazquez, J.; Savaniu, C.; Marrero-Lopez, D.; Zhou, W.; Irvine, J. T. S. *Nature* **2006**, *439*, 568.
(4) Huang, Y. H.; Dass, R. I.; Xing, Z. L.; Goodenough, J. B. *Science* **2006**, *312*, 254.
(5) Mitchell, R. H. *Perovskites: Modern and Ancient*; Almaz Press Inc.: Thunder Bay, ON, 2002.
(6) Knapp, M. C.; Woodward, P. M. *J. Solid State Chem.* **2006**, *179*, 1076.
(7) Brixner, L. H. *J. Am. Chem. Soc.* **1958**, *80*, 3214.
(8) Spitsyn, V. I.; Ippolitova, E. A.; Kovba, L. M.; Lykova, L. N.; Leshchenko, P. P. *Russ. J. Inorg. Chem.* **1982**, *27* (4), 464.
(9) Leshchenko, P. P.; Lykova, L. N.; Kovba, L. M.; Ippolitova, E. A. *Russ. J. Inorg. Chem.* **1982**, *27* (5), 721.
(10) Browall, K. W.; Muller, O.; Doremus, R. H. *Mater. Res. Bull.* **1976**, *11*, 1475.
(11) Lecomte, J.; Loup, J. P.; Hervieu, M.; Raveau, B. *Phys. Status Solidi* **1981**, *A65*, 743.
(12) Neiman, A. Y.; Podkorytov, A. L.; Zhukovskii, V. M. *Phys. Status Solidi* **1987**, *A101*, 371.
(13) Turrillas, X.; Sellars, A. P.; Steele, B. C. H. *Solid State Ionics* **1988**, *28–30*, 465.
(14) Glöckner, R.; Neiman, A.; Larring, Y.; Norby, T. *Solid State Ionics* **1999**, *125*, 369.
(15) Animitsa, I.; Neiman, A.; Sharafutdinov, A.; Nochrin, S. *Solid State Ionics* **2000**, *136–137*, 265.
(16) Animitsa, I.; Nieman, A.; Titova, S.; Kochetova, N.; Isaeva, E.; Sharafutdinov, A.; Timofeeva, N.; Colomban, P. *Solid State Ionics* **2003**, *156*, 95.
(17) Caldes, M. T.; Deniard, P.; Zou, X. D.; Marchand, R.; Diot, N.; Brec, R. *Micron* **2001**, *32*, 497.
(18) Deniard, P.; Caldes, M. T.; Zou, X. D.; Diot, N.; Marchand, R.; Brec, R. *Int. J. Inorg. Mater.* **2001**, *3*, 1121.
(19) Levin, I.; Chan, J. Y.; Scott, J. H.; Farber, L.; Vanderah, T. A.; Maslar, J. E. *J. Solid State Chem.* **2002**, *166*, 24.

10.1021/cm703396t CCC: $40.75
Published on Web 03/15/2008

2. Experimental Section

Samples of $Sr_{6-2x}Nb_{2+2x}O_{11+3x}$ with $x = 0.103$, 0.143, 0.185, 0.231, 0.280, and 0.333 were prepared by solid-state reaction from the nominal mixtures of high purity $SrCO_3$ (99.994%, Alfa Aesar) and Nb_2O_5 (99.9985%, Alfa Aesar) via ball-milling in ethanol. The compositions correspond to Sr:Nb ratios of 10.5:4, 10:4, 9.5:4, 9:4, 8.5:4, and 8:4, respectively. These powders were pressed into pellets, heated in air at 1273 K for 24 h, and at 1523 K for 72 h with intermediate grinding and pressing. With the aim of performing some conductivity measurements, some parts of the products were reground, pressed into disks with a CIP (cold isostatic pressing) pressure of 300 MPa, and sintered at 1673 K in air for 16 h. A relative density higher than 90% of the theoretical value was obtained. The heating and cooling rates were 200 K/h for all the heat treatment. For electrical measurements, the sintered pellets were cut into parallelepiped of ca. $3 \times 3 \times 15$ mm^3 dimensions. ICP (inductively coupled plasma) elemental analyses were carried out using a Perkin-Elmer Optima 5300DV, confirming that the compositions for the final products were similar to the nominal compositions with deviations of 1.3–4.2% (see the Supporting Information for details).

The powder X-ray diffraction (XRD) data were collected at room temperature on a Bragg–Brentano diffractometer (Bruker-AXS Advance D8) with a Cu X-ray tube, a focusing primary Ge (111) monochromator (λ= 1.5406 Å) and a position sensitive Väntec detector with a detector slit of 6° over an angular range of $10° \leq 2\theta \leq 145°$ with a step of 0.016662° and a total measurement time of 5 h. Neutron powder diffraction measurements for the selected samples ($x = 0.103$, 0.185, and 0.280) were performed at room temperature in air using HANARO HRPD equipment with a 32-He-3 Multidetector systems and a Ge (331) monochromator operated by the Korea Atomic Energy Institute, Daejeon, Korea. The data were collected with a wavelength of 1.8341 Å over the 2θ range of 10–150° with a step of 0.05° and a total measurement time of 3 h. The sample amounts used were 10–15 g. The combined Rietveld refinement of X-ray and neutron diffraction data was performed using the profile refinement program GSAS.[20] The refinement parameters were scale factors, background, unit-cell parameters, peak profile coefficients, extinction coefficient (XRD only), atomic coordinates, thermal parameters, and occupancies for Sr2, Nb2, O1, and O2.

A four-probe d.c. method was applied to measure the electrical conductivities as functions of temperature and oxygen partial pressure under dry and wet air. Electrodes were formed by applying Pt-paste. When a value for conductance of a specimen varied by less than 1% in one hour or so at a given condition, it was taken to be the corresponding equilibrium value. The oxygen partial pressure in the range of $-20 \leq \log(P_{O_2}/\text{atm}) \leq 0$ was controlled by flowing either N_2/O_2 or CO/CO_2 gas mixtures and monitored by a zirconia-based electrochemical cell. The wet air was obtained by bubbling air through distilled water at room temperature.

3. Results and Discussion

3.1. Powder X-ray and Neutron Analysis. Room-temperature XRD patterns for the series of compounds $Sr_{6-2x}Nb_{2+2x}O_{11+3x}$ ($x = 0.103$, 0.143, 0.185, 0.231, 0.280, and 0.333) are presented on a magnified scale in Figure 1. It should be mentioned that $Sr_6Nb_2O_{11}$ ($x = 0$)[8,9] is known to have a temperature dependence of phase stability and a closely related, but more subtle crystal structure compared to the other compounds reported here. We have also found in the XRD pattern that $Sr_{6-2x}Nb_{2+2x}O_{11+3x}$ with $x = 0.0667$ displayed an unidentified but obviously different structure type with a bigger unit cell from the others. Further crystallographic characterization is necessary, and will not be discussed in this paper. All patterns indicated a typical double-perovskite type structure with a space group of $Fm\bar{3}m$. Notably the patterns show diffuse intensity in the form of bumpy backgrounds, which are stronger in the neutron diffraction patterns (Figure 4b), implying a strong contribution from the oxygen subcell as reported for $Sr_{5.6}Ta_{2.4}O_{11.6}$[17,18] and $Sr_4Nb_2O_9$.[19] Eventually, the analysis of such diffuse scattering must be conducted for a better understanding of the crystal structure and properties. However, we have focused on Bragg reflections that contain valuable information on the average structure that was determined and refined in this work.

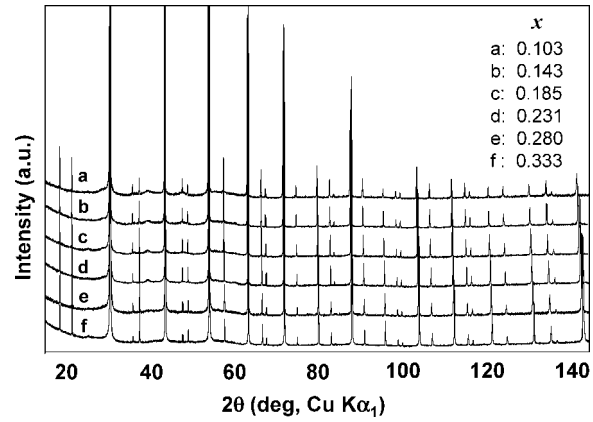

Figure 1. X-ray diffraction patterns for $Sr_{6-2x}Nb_{2+2x}O_{11+3x}$ ($0.103 \leq x \leq 0.333$) at room temperature on a magnified scale for clarity.

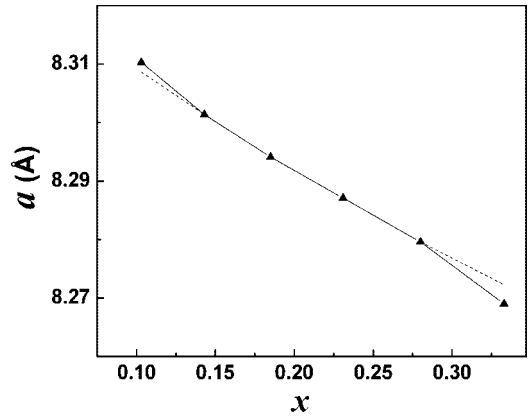

Figure 2. Variation of unit-cell parameters with composition x for $Sr_{6-2x}Nb_{2+2x}O_{11+3x}$ ($0.103 \leq x \leq 0.333$).

The $Sr_{6-2x}Nb_{2+2x}O_{11+3x}$ unit-cell parameters decrease linearly with x increase following the Vegard's law as shown in Figure 2. It demonstrates that Sr and Nb form a good solid solution in the structure. The variation is in agreement with the radius difference between Sr^{2+} ($r = 1.18$ Å in 6-fold coordination) and the relatively smaller Nb^{5+} ($r = 0.64$ Å) ions.[21]

(20) Larson, A. C.; Von Dreele, R. B. *General Structure Analysis System (GSAS)*; Los Alamos National Laboratory Report LAUR 86–748; Los Alamos National Laboratory: Los Alamos, NM, 2000.

(21) Shannon, R. D. *Acta Crystallogr.* **1976**, *A32*, 751.

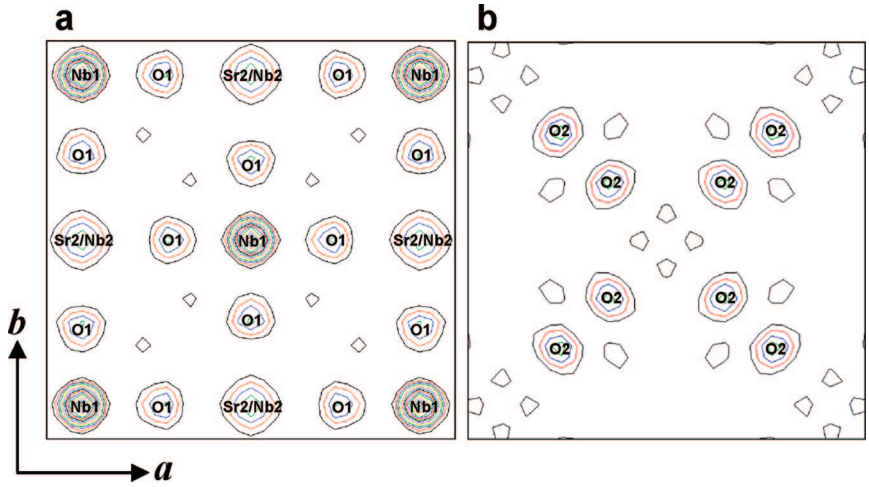

Figure 3. (001) sections of (a) observed and (b) difference Fourier synthesis maps (neutron) at $z = 0$ for $Sr_{6-2x}Nb_{2+2x}O_{11+3x}$ ($x = 0.103$) at the refinement stage prior to the location of the interstitial oxygen (O2) atom.

The compounds characterized by X-ray and neutron diffraction ($x = 0.103$, 0.185, and 0.280) were first analyzed since the neutron diffraction data would be significant for a reliable refinement of oxygen atoms. The typical cubic cryolite structure was used as a starting model, where the metal sites were fully occupied and the pure Nb and the mixed Sr/Nb sites form a rock-salt type ordering. Because Sr and Nb have almost identical X-ray atomic scattering factors ($\Delta Z = 2$) and neutron scattering lengths ($b_{c,Sr} = 7.02$, $b_{c,Nb} = 7.054$), refinement of the site occupancies for Sr and Nb was practically impossible. Nevertheless, due to large size difference between Sr and Nb, bond distances to oxygen could be used for identification and refinement. In all cases, the refinements produced poor reliability factors and extremely small (for Nb1) or large (for the other atoms) ADPs, suggesting that the model of the cubic cryolite-like structure is only approximate. However, careful examination of the diffraction patterns at high angles up to ~150° in 2θ did not show any evidence of splitting or asymmetry of the cubic reflections. Thus, we concluded that the cubic symmetry was still retained for the average crystal structure. Similar phenomena have been observed for $Sr_{5.6}Ta_{2.4}O_{11.6}$ and $Sr_4Nb_2O_9$. For the former case, nonharmonicity on ADPs in a Rietveld calculation was used to successfully explain the observed neutron diffraction pattern and the existence of a micro domain determined by HREM (high-resolution electron microscope).[17,18] For the latter case, split-atom models were applied to obtain improved refinement results. The A-site Sr and oxygen (O1) were shifted slightly by less than 0.4 Å from the ideal 8*c* and 24*e* sites to 32*f* and 96*k* (or 192*l*), respectively.[19] A similar oxygen disorder was also observed in some double perovskites, such as Pb_2CoWO_6[22] and Pb_2MgWO_6.[23] We also applied the split-atom model to the series of compounds. The fits were improved, however, the profiles and ADPs of the refinement results were not satisfactory, and still exhibited poor reliability factors ($R_p/wR_p = 6.54/10.35\%$ for example with $x = 0.103$) and very large ADPs, except for Nb1. At this point, the observed and difference Fourier synthesis maps were calculated as shown in Figure 3, using the subprograms FOURIER and FORPLOT embedded in GSAS.[20] Interestingly, interstitial oxygens (O2) are clearly observed in the difference Fourier map. The distances from Nb1 to the two oxygen positions (O1 and O2) are similar. On the basis of these maps, we could build a new structural model where the oxide ions are distributed statistically over the normal (O1) and the interstitial (O2) positions.

The partial occupancies of the two oxygen sites were refined with a constraint that would satisfy the charge neutrality condition of the compounds. The site occupancies for Sr2/Nb2 were also released for refinement with a restraint that the overall Sr/Nb ratios were to be maintained to the nominal composition. The occupancies were very close to 100%, with a deviation of less than 1%, hence fixed to the unity, except for the composition $x = 0.333$, which exhibited a small deficiency of about 3%. This is probably because the composition $x = 0.333$ corresponds to the Nb-richest composition and the highest oxygen total occupancy, which would make the atoms in the structure the most crowded among the series, and thus might induce a small defect in the metal site. Refinement of the anisotropic displacement parameters for O2 was unstable, probably because of very small occupancies (8.5%–15.4%), thus only isotropic parameters were refined. For the compounds with X-ray data only, isotropic displacement parameters for O1 and O2 were fixed at 0.06 $Å^2$, which is roughly an average value from the results of the combined refinements of X-ray and neutron cases. The refinement profile fits were dramatically improved for all the cases ($R_p/wR_p = 4.02/5.63\%$ for example with $x = 0.103$). More plausible ADPs were also observed, but still exhibited larger values as compared to those for normal perovskite-type oxides. The final profile fits are shown in Figure 4 for $x = 0.103$. The refinement results and selected bond lengths for $x = 0.103$, 0.185, and 0.230 are given in Tables 1 and 2, respectively. The profile fits for the other compounds and the refinement results from X-ray data only ($x = 0.143$, 0.231, and 0.333) are given in the Supporting Information.

(22) Baldinozzi, G.; Sciau, P.; Lapasset, J. *Phys. Status Solidi* **1992**, *A133*, 17.
(23) Baldinozzi, G.; Sciau, P.; Pinot, M.; Grebille, D. *Acta Crystallogr., Sect. B* **1995**, *51*, 668.

Table 1. Atomic Coordinates, Unit-Cell Parameters, Site Occupancies, Isotropic Displacement Parameters and Reliability Factors for $Sr_{6-2x}Nb_{2+2x}O_{11+3x}$ from the Combined Rietveld Refinement of Powder X-ray and Neutron Diffraction Data (x = 0.103, 0.185, and 0.280) at Room Temperature (SG = $Fm\bar{3}m$, No. 225, Z = 2)

atom	site	x	y	z
Sr1	8*c*	¼	¼	¼
Nb1	4*a*	0	0	0
Sr2/Nb2	4*b*	½	½	½
O1	24*e*	x_p	0	0
O2	48*h*	0	y_p	y_p

composition, x	0.103	0.185	0.280
Sr:Nb ratio	10.5:4	9.5:4	8.5:4
a (Å)[a]	8.3103(1)	8.2941(1)	8.2796(1)
V (Å^3)[a]	573.91(1)	570.57(1)	567.59(1)
x_p for O1	0.2391(2)	0.2395(2)	0.2387(2)
y_p for O2	0.1654(3)	0.1646(3)	0.1635(3)
		occupancy[b]	
Sr2/Nb2	0.90/0.10	0.81/0.19	0.72/0.28
O1	0.635(1)	0.715(2)	0.816(2)
O2	0.154(1)	0.124(1)	0.085(1)
		U_{iso} ($\times 10^2$ Å^2)[c]	
Sr1	7.76(3)	5.96(2)	4.80(2)
Nb1	2.19(2)	1.66(2)	1.40(2)
Sr2/Nb2	11.63(6)	8.69(4)	6.97(4)
O1[d]	6.94(7)	6.88(6)	7.49(5)
O2[e]	5.18(10)	4.06(12)	2.42(13)
		R_p/wR_p (%)[f]	
X-ray	5.80/7.74	4.22/5.66	5.18/6.66
neutron	3.27/4.46	2.89/3.89	3.09/4.10
total	4.02/5.63	3.44/4.68	3.75/5.05
χ^2	4.44	4.32	3.49

[a] Estimated standard deviations are denoted as 1 when the values are less than 1. [b] Sr1 and Nb1 sites are fully occupied with occupancy factor of 1. [c] $U_{iso} = (U_{11} + U_{22} + U_{33})/3$. For metals, $U_{11} = U_{22} = U_{33}$, $U_{12} = U_{13} = U_{23} = 0$. For O1, $U_{22} = U_{33}$, $U_{12} = U_{13} = U_{23} = 0$. [d] [$U_{11}$, U_{22}]($\times 10^2$ Å^2) = [3.07(8), 8.88(7)], [3.05(7), 8.79(6)], and [3.26(6), 9.61(5)] for x = 0.103, 0.185, and 0.280, respectively. [e] O2 was refined isotropically. [f] $R_p = 100\Sigma|I_o - I_c|/\Sigma\Delta I_o|$; $wR_p = 100(\Sigma w|I_o - I_c|^2/\Sigma w|I_o|^2)^{1/2}$; $\chi^2 = 100\Sigma w|I_o - I_c|^2/(N_{obs} - N_{var.})$.

Table 2. Selected Interatomic Distances (Å) in $Sr_{6-2x}Nb_{2+2x}O_{11+3x}$ (x = 0.103, 0.185, and 0.280) at Room Temperature

	x		
bond	0.103	0.185	0.280
Sr1−O1	2.939(1) × 12	2.934(1) × 12	2.928(1) × 12
Sr1−O2	2.303(1) × 12	2.303(2) × 12	2.304(2) × 12
Nb1−O1	1.987(2) × 6	1.987(2) × 6	1.976(1) × 6
Nb1−O2	1.944(3) × 12	1.931(3) × 12	1.914(4) × 12
M−O1[a]	2.168(2) × 6	2.160(2) × 6	2.164(1) × 6
M−O2	3.102(1) × 24	3.099(1) × 24	3.098(1) × 24
O1−O2	1.505(1)	1.500(1)	1.490(1)
O2−O2	1.944(3)	1.931(3)	1.914(4)
	1.988(6)	2.003(7)	2.026(8)

[a] M = Sr2/Nb2.

3.2. Crystal Structure. The unit cell of $Sr_{6-2x}Nb_{2+2x}O_{11+3x}$ is shown in Figure 5, where MO_6 (M = Sr2/Nb2) is drawn as a hatched one. The Nb1 is surrounded by oxygen and anionic vacancies statistically distributed over the two sites (six equivalent O1's and 12 equivalent O2's) to form eighteen partially occupied oxygen atoms, which may be represented as a $Nb^{(1)}O_{18/3}$ polyhedron to emphasize the total number of oxygen positions (18) and three times (3) the normal coordination surrounding Nb1. A very similar local environment was observed in $Ba_{11}W_4O_{23}$ or $(Ba_{1.75}\square_{0.25})(BaW)O_{5.75}\square_{0.25}$ with 4 × 4 × 4 superstructure of a simple perovskite, where the A-site vacancies are ordered, the B-site

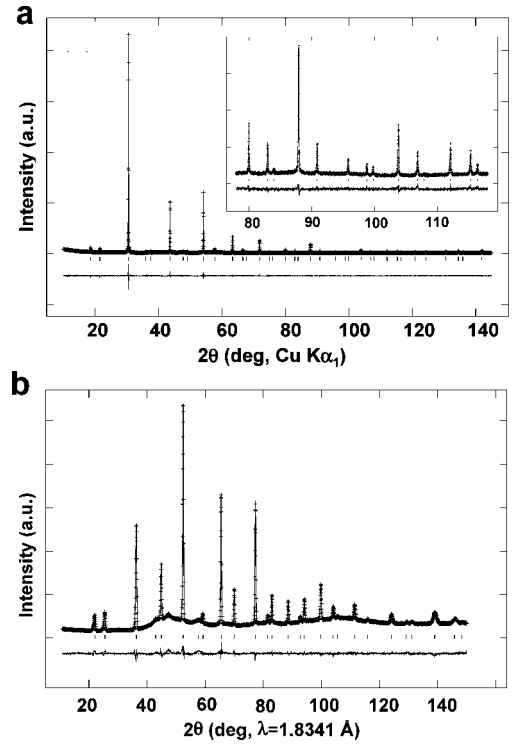

Figure 4. Combined (a) X-ray and (b) neutron Rietveld refinement profiles for $Sr_{6-2x}Nb_{2+2x}O_{11+3x}$ (x = 0.103) recorded at room temperature. The cross line marks experimental points and the solid line is the calculated profile. The lower trace shows the difference curve, and the ticks denote expected peak positions. The inset shows the high angle data in details.

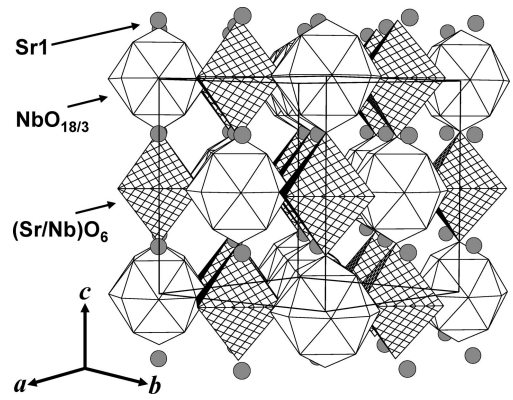

Figure 5. (110) view of the crystal structure of $Sr_{6-2x}Nb_{2+2x}O_{11+3x}$. MO_6 (M = Sr2/Nb2) are shown as hatched octahedra, and $Nb^{(1)}O_{18/3}$ are shown as white polyhedra. Sr1 is shown as gray spheres. The unit cell is outlined.

is fully occupied with a 1:1 ordering of Ba and W ions, the anionic vacancies are disordered, and half-the tungsten ions have a normal WO_6 octahedron, but the other half-have an unusual $WO_{18/3}$ environment.[24]

A slab of (001) plane around z = 0 with a thickness of ~5 Å is shown in Figure 6. The $Nb^{(1)}O_{18/3}$ polyhedra display 1D arrangements along [110] and [1–10] directions in the slab and along four other equivalent directions in the 3D network of the crystal structure. The closest interpolyhedral O−O contact is O2−O2 with a distance of 1.65–2.026 Å, which is too close to be occupied simultaneously, as indicated by the partial occupancy of less than 15.4% for all cases. It

(24) Hong, S.-T. *J. Solid State Chem.* **2007**, *180*, 3039.

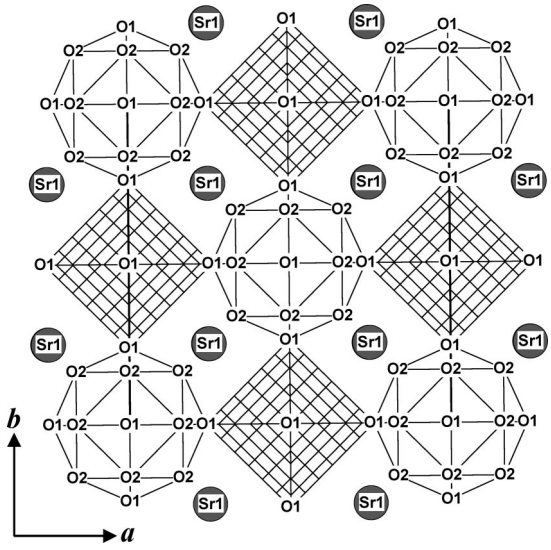

Figure 6. Slab of the (001) plane around $z = 0$ with a thickness of ~5 Å for $Sr_{6-2x}Nb_{2+2x}O_{11+3x}$ ($0.103 \le x \le 0.333$). MO_6 (M = Sr2/Nb2) are shown as a hatched octahedron. The lower corner of the slab is a $Nb^{(1)}O_{18/3}$ polyhedron.

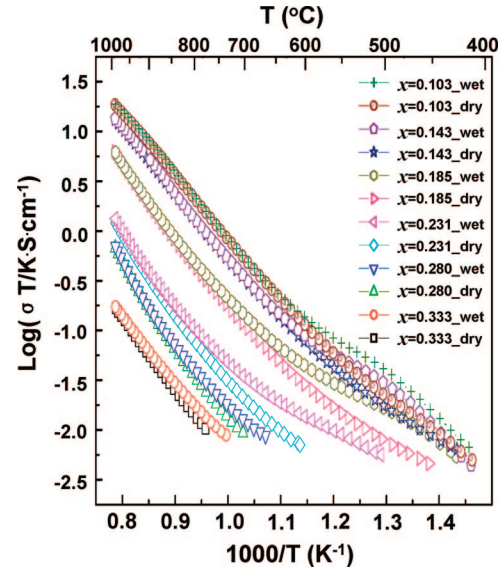

Figure 7. Arrhenius plots showing the temperature and composition dependencies of electrical conductivities for $Sr_{6-2x}Nb_{2+2x}O_{11+3x}$ ($0.103 \le x \le 0.333$) under dry and wet air.

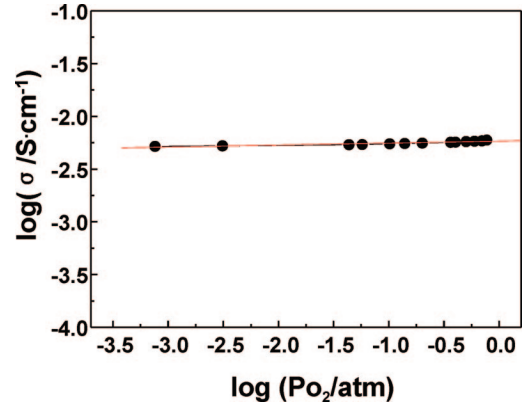

Figure 8. Electrical conductivity of $Sr_{6-2x}Nb_{2+2x}O_{11+3x}$ ($x = 0.103$) vs oxygen partial pressure at 1170 K under dry atmosphere.

appears that such O2 sites are on the oxide ion migration pathway in the structure, however, such O2–O2 hopping would be hindered by the A-site Sr1 ions located between $Nb^{(1)}O_{18/3}$ polyhedra. This will likely depress the oxide ion conductivity. On the other hand, $Ba_{11}W_4O_{23}$ has similar 1D arrangements of $WO_{18/3}$ polyhedra, but half of such hindering A-site cations are vacancies, which are ordered in between two adjoining $WO_{18/3}$.

O1 lies midway between the two B-site metals of Nb1 and Sr2/Nb2. The distances of d(Nb1−O1) and d(O1−Sr2/Nb2) are 1.989 and 2.168 Å, respectively, for example, with $x = 0.103$. The former is slightly shorter but the latter is much shorter than the expected values from their ionic radii sums, 2.04 and 2.526 Å (weighted by 90% Sr and 10% Nb), respectively.[21] This makes the O1 position very unstable due to the heavy stress of the structure, probably causing some oxygen atoms in the O1 site to be driven to the interstitial O2 site. As a consequence, the structure becomes a little more relaxed: the distance from O2 to nearest strontium Sr1 is 2.303 Å, which is still shorter than the ionic sum 2.58 Å,[21] but longer than the distance from O1 to nearest strontium Sr2/Nb2, 2.168 Å. The short distances between oxygen and strontium must be highly responsible for the large ADPs for all atoms, except Nb1. This conforms to the fact that the ADPs for Sr1 and Sr2/Nb2 atoms decrease significantly with x increase or Sr content decrease as shown in Table 1.

The bond valence sums[25] calculated with the program Valence[26] for Sr1, Nb1, Sr2/Nb2, O1, and O2 for the compound with $x = 0.103$, for example, are 1.95, 4.79, 3.43, 2.08, and 2.26 v.u., respectively. The values for the other compounds are similar and reasonably match the expected ion charges.

3.3. Electrical Conductivity. The total conductivities are shown in Figure 7 for $Sr_{6-2x}Nb_{2+2x}O_{11+3x}$, as measured under dry (log $P_{H_2O} = -3.9$) or wet air (log $P_{H_2O} = -1.5$). The conductivities in air were reproducible during several cycles of cooling and heating for all compounds. In contrast, the conductivities at high temperature (e.g., 1173K) under reducing atmospheres could not be measured reproducibly because the conductivity values fluctuated. This is because some portion of the samples was decomposed into a mixture of $SrNb_4O_6$ and unidentified phases under N_2/O_2 gas, except for the compound with $x = 0.103$, or into $SrCO_3$ under CO/CO_2 gas.

The total conductivity as a function of oxygen partial pressure at 1173K in the range of $-4 \le \log(P_{O_2}) \le 0$ is shown in Figure 8 for the compound with $x = 0.103$. The conductivity appears to increase with increasing P_{O_2}, but the rate is small enough ($|\partial \log \sigma / \partial \log P_{O_2}| < 1/35$) to neglect. We may thus, conclude that the present conductivity is essentially ionic, at least, for the compound with $x = 0.103$. Previous studies also showed that the ionic contribution was found to dominate over the electronic contribution in the wide ranges of oxygen partial pressures for the compounds with $x = 0.0667$[12] and $x = 0.2733$.[11] Therefore, it is likely that

(25) Brown, I. D.; Altermatt, D. *Acta Crystallogr., Sect. B* **1985**, *41*, 244.
(26) Brese, N. E.; O'Keeffe, M. *Acta Crystallogr., Sect. B* **1991**, *47*, 192.

the total conductivities measured in air for the compounds presented here were predominantly due to ionic.

The total conductivity increases with higher Sr content (smaller x) and higher oxygen defects. The activation energy 1.23 eV, for example with $x = 0.103$, is similar to the value (1.19 eV) reported for $Sr_6Nb_2O_{11}$[13] and higher than the reported values (0.7–1.0 eV) for the conventional electrolytes $Gd_2Ti_2O_7$,[27] YSZ ($Y_{0.148}Zr_{0.852}O_{1.926}$),[28] $La_{0.9}Sr_{0.1}Ga_{0.8}Mg_{0.2}O_{3-\delta}$,[29] and $Gd_{0.18}Ce_{0.82}O_{2-\delta}$.[30] Water vapor enhances the conductivity below ca. 900 K and apparently reduces its activation energy, displaying a characteristic proton conductor.

Isothermal conductivity enhancement is greater than 2 orders of magnitude for different x's. For example, the conductivity increases from 1.73×10^{-4} for $x = 0.333$ to 1.85×10^{-2} S cm^{-1} for $x = 0.103$ at 1273 K. Interestingly, the conductivity is enhanced with a lower total oxygen content but higher occupancy in the interstitial oxygen (O2) site.

Conclusions

Crystal structure investigation on perovskite-related ionic conductors $Sr_{6-2x}Nb_{2+2x}O_{11+3x}$ ($0.103 \leq x \leq 0.333$) using a combined powder X-ray and neutron diffraction method resulted in a new structural model with interstitial oxide ions, which appear to be on the oxide ion conduction pathway. The new structural model provides an important basis for understanding the properties of such cryolite-related ion conducting materials.

Acknowledgment. The authors would like to thank Dr. Y. N. Choi in the Korea Atomic Energy Institute, Daejeon, Korea, for his help with neutron powder diffraction measurements.

Supporting Information Available: Tables of refined parameters, atomic coordinates, and selected interatomic distances for $Sr_{6-2x}Nb_{2+2x}O_{11+3x}$ ($x = 0.143$, 0.231, 0.333). Table of ICP elemental analysis results. XRD patterns after sintering at 1673 K. Comparison of the unit-cell parameters with previous works. Rietveld refinement profiles for the compounds with $x = 0.143$, 0.185, 0.231, 0.280, and 0.333 (PDF). This material is available free of charge via the Internet at http://pubs.acs.org.

CM703396T

(27) Kramer, S. A.; Tuller, H. L. *Solid State Ionics* **1995**, *82*, 15.
(28) Yoo, H.-I.; Hwang, J.-H. *J. Phys. Chem. Solids* **1992**, *53*, 973.
(29) Kim, J.-H.; Yoo, H.-I. *Solid State Ionics* **2001**, *140*, 105.
(30) Ahlgren, E. O.; Poulsen, F. W. *J. Phys. Chem. Solids* **1996**, *57* (5), 589.